Research Article

Ömer Sercik*, Steven Abrams and Anneleen Verhasselt

Bernstein-based nonparametric estimation of the cross ratio function under univariate right censoring

https://doi.org/10.1515/demo-2025-0023
Received December 8, 2025; accepted May 23, 2026; published online August 3, 2026

Abstract: Bivariate time-to-event data often arise in various fields, including medicine, engineering, and economics, where understanding the association between two survival times is crucial. Traditional global association measures like Spearman's rho and Kendall's tau provide an average assessment, but fail to capture how association evolves over time. Local association measures, on the other hand, including the so-called cross ratio function (CRF), have been proposed to look at the association in more detail. This paper introduces a novel nonparametric estimator for the CRF applicable for univariate right-censored data, relying on Bernstein polynomials to obtain a smooth estimate of the bivariate survival copula, its partial derivatives, and the copula density. The proposed estimator's finite-sample performance is evaluated through an elaborate simulation study and applied to real-life data, highlighting its practical utility and setting the stage for future research on local association in survival analysis.

Keywords: Bernstein polynomials; survival copula; local association

MSC 2020: 62G05; 62N02; 62H20

1 Introduction

Nowadays bivariate time-to-event data, of primary focus here, are collected in various domains. For example, in a medical context, the occurrence of a disease in two potentially related individuals (e.g., father-son, siblings, twin or household members, colleagues, etc.) could be studied. However, this is not restricted to medical examples, as bivariate time-to-event data naturally arise in different fields such as engineering (e.g., reliability of mechanical devices), biology (e.g., extinction of closely related species), economics (e.g., time to bankruptcy and asset liquidation among firms in financial distress), insurance (e.g., life or health insurance claims for partners), to name a few. Modeling time-to-event data is often complicated by the typical presence of (right) censoring, thereby preventing the event times for some subjects from being exactly known. Right-censored data arise, for

***Corresponding author: Ömer Sercik**, Data Science Institute, Interuniversity Institute for Biostatistics and statistical Bioinformatics, Hasselt University, Agoralaan Gebouw D, Diepenbeek, 3590, Limburg, Belgium, E-mail: omer.sercik@uhasselt.be
Steven Abrams, Data Science Institute, Interuniversity Institute for Biostatistics and statistical Bioinformatics, Hasselt University, Agoralaan Gebouw D, Diepenbeek, 3590, Limburg, Belgium; and Global Health Institute, Department of Family Medicine and Population Health, University of Antwerp, Universiteitsplein 1, Wilrijk, 2610, Antwerp, Belgium. https://orcid.org/0000-0001-7353-9304
Anneleen Verhasselt, Data Science Institute, Interuniversity Institute for Biostatistics and statistical Bioinformatics, Hasselt University, Agoralaan Gebouw D, Diepenbeek, 3590, Limburg, Belgium

example, when study subjects do not experience the event of interest prior to the end of the study (administrative censoring), subjects are lost to follow-up, or withdraw themselves from the study. Next to right censoring, other types of censoring could occur (i.e., interval-censored or left-censored data).

In case of bivariate time-to-event data, one is typically interested in assessing the strength of association between two survival times T_1 and T_2. Several methods exist in the literature to describe the (global) association between two (event time) random variables of which the most famous examples are rank-based measures like Spearman's rho (Spearman 1904) and Kendall's tau (Kendall 1948). These only provide an average perspective on association throughout the bivariate domain spanned by the random variables T_1 and T_2. In the above-mentioned examples of bivariate time-to-event data, it is interesting to assess how the association evolves over time. Similarly to the existence of several global association measures, local ones have been proposed in the literature as well. Examples of local association measures are time-dependent versions of Kendall's tau (Oakes 1989) and the odds ratio (see, e.g., Anderson et al. 1992). Next to the local Kendall's tau and the local odds ratio, other measures have been proposed in the literature on the analysis of bivariate time-to-event data, including the expected residual life (Anderson et al. 1992), the risk ratio (Abrams et al. 2022), and the average relative risk (Fan et al. 2000), among other measures.

In this manuscript, we focus on the estimation of the cross ratio function (CRF) as a local association measure, initially introduced by Clayton (1978) and defined as the ratio of the conditional hazards of event one, either given that event two occurs at a specific time point t_2, or it happens beyond t_2. The CRF therefore provides a detailed local perspective on association between the event times. Parametric, semi-parametric and nonparametric estimators for the CRF have been proposed for both uncensored and right-censored data, however, some under strong assumptions or exhibiting a rough behavior. More recently, Bernstein-based CRF estimation has been considered in the uncensored case (Abrams et al. 2020, 2024), thereby building on desirable theoretical bias properties of Bernstein smoothing methods (see, e.g., Janssen et al. 2012, 2014, 2016). Although these studies focus on fully observed data, the literature has extended the estimation of the CRF to censored data. Hu et al. (2011) proposed a polynomial model for the CRF, whereas Nan et al. (2006) introduced a piecewise constant CRF model, both in the context of bivariate right-censored data. In contrast, Hu et al. (2014) and Kim and Lee (2021) proposed CRF estimators for left-truncated and interval-censored data, respectively.

In this paper, we introduce a new nonparametric estimator for the CRF for bivariate time-to-event data for which some observations are right-censored using a univariate censoring process. More specifically, a plug-in estimator is defined in Section 2, relying on Bernstein-based estimators for the different components of the CRF, i.e., the survival copula, its partial derivatives, and the copula density. This extends the approach considered by Dib et al. (2021) when estimating the copula under one-component censoring (i.e., only one event subject to right censoring). In Section 3, we perform an extensive simulation study to assess the performance of the newly introduced CRF estimator. In particular, we study the performance in terms of the sample size, percentage of censoring and the global association of Kendall's tau, for different dependence structures. Moreover, the new estimator is applied to a real life data application on Diabetic Retinopathy data in Section 4. We highlight some challenges and avenues for future research in Section 5. Furthermore, the appendix presents a fully parametric estimator of the CRF based on maximum likelihood estimation. Finally, the Supplementary Material of this manuscript contains some additional results of our nonparametric estimator.

2 Materials and methods

We first introduce the terminology and notation used throughout the text in Section 2.1. In Section 2.2, we provide the formal definition of the CRF and provide information about its different ingredients, and finally, we propose our estimator in Section 2.3.

2.1 Terminology and notation

Consider two non-negative random variables $T_j \geq 0$, $j = 1, 2$, with joint survival function and cumulative distribution function (CDF) denoted by $S(t_1, t_2) = P(T_1 > t_1, T_2 > t_2)$ and $F(t_1, t_2) = P(T_1 \leq t_1, T_2 \leq t_2)$ (with $t_1, t_2 \geq 0$), respectively. Here we focus our attention to independent univariate right censoring described by the censoring variable $C \geq 0$ with corresponding survival function $S_C(c) = P(C > c)$ (with $c \geq 0$). Furthermore, let $Y_1 = \min(T_1, C)$ and $Y_2 = \min(T_2, C)$ with censoring indicators $\Delta_1 = \mathbb{I}(T_1 \leq C)$ and $\Delta_2 = \mathbb{I}(T_2 \leq C)$ for T_1 and T_2, respectively, and $\Delta_C = 1 - \Delta_1\Delta_2$ indicating censoring of C if T_1 and T_2 are both observed. Assuming independence between (T_1, T_2) and C, we have that the joint survival function of T_1 and T_2 is

$$S(t_1, t_2) = \frac{S_Y(t_1, t_2)}{S_C(t_1 \vee t_2)},$$

where $S_Y(y_1, y_2) = P(Y_1 > y_1, Y_2 > y_2)$ (with $y_1, y_2 \geq 0$) is the joint survival function of (Y_1, Y_2) and $a \vee b$ denotes the maximum of a and b.

In general, we define the upper endpoint of the support of a random variable X with CDF $F_X(x)$ by $t_X = \inf\{x : F_X(x) = 1\}$. Therefore, let t_{T_1}, t_{T_2} and t_C represent the upper endpoints of the supports of T_1, T_2 and C, respectively. The upper endpoint of the supports of Y_1 and Y_2 are denoted by $t_{Y_1} = \min(t_{T_1}, t_C)$ and $t_{Y_2} = \min(t_{T_2}, t_C)$, respectively.

According to Sklar's theorem (Sklar 1959), the joint survival function $S(t_1, t_2)$ can be expressed in terms of a (survival) copula function applied to the marginal survival functions of T_1 and T_2, i.e., $S_1(t_1) = P(T_1 > t_1)$ and $S_2(t_2) = P(T_2 > t_2)$, respectively. In particular, there exists a unique function C (the survival copula) such that

$$S(t_1, t_2) = C[S_1(t_1), S_2(t_2)]. \tag{1}$$

For continuous marginals $S_1(t_1)$ and $S_2(t_2)$, we can also write

$$C(u_1, u_2) = S\left[S_1^{-1}(u_1), S_2^{-1}(u_2)\right],$$

with $0 \leq u_1, u_2 \leq 1$. Hereafter we will refer to C as the copula function, thus suppressing the *survival* aspect for simplicity. The reader is referred to Nelsen (2007) for a detailed account of copula functions.

2.2 Cross ratio function

The cross ratio function is a local association measure introduced by Clayton (1978) to analyze the familial tendency in chronic disease incidence among parents and their offspring and between siblings. The CRF is defined as (Clayton 1978; Oakes 1989):

$$\theta(t_1, t_2) = \frac{\lambda_1(t_1 \mid T_2 = t_2)}{\lambda_1(t_1 \mid T_2 > t_2)},$$

where $\lambda_1(t_1 \mid T_2 = t_2)$ and $\lambda_1(t_1 | T_2 > t_2)$ are the conditional hazard functions of T_1 given $T_2 = t_2$ and $T_2 > t_2$, respectively. Note that the measure is symmetric in nature in the sense that the role of T_1 and T_2 is interchangeable. Some straightforward calculations show that

$$\theta(t_1, t_2) = \frac{\lambda_2(t_2 \mid T_1 = t_1)}{\lambda_2(t_2 \mid T_1 > t_1)},$$

with similar definitions for the conditional hazard functions of T_2, given the first event occurring at or beyond t_1. For $\theta(t_1, t_2) > 1$, $\theta(t_1, t_2) < 1$ or $\theta(t_1, t_2) = 1$, we have a positive, negative or no association between T_1 and T_2 in (t_1, t_2), respectively.

Alternatively, the CRF can be expressed in terms of the joint survival function $S(t_1, t_2)$, and its partial derivatives:

$$\theta(t_1, t_2) = \frac{S(t_1, t_2)\, S^{(1,2)}(t_1, t_2)}{S^{(1)}(t_1, t_2)\, S^{(2)}(t_1, t_2)},$$

using the notation (for any function $g(x_1, x_2)$ and $k = 1, 2$):

$$g^{(k)}(x_1, x_2) = \frac{\partial g(x_1, x_2)}{\partial x_k},$$

$$g^{(1,2)}(x_1, x_2) = \frac{\partial^2 g(x_1, x_2)}{\partial x_1 \partial x_2}.$$

Note that $S^{(1,2)}(t_1, t_2)$ is equal to the joint density function $f(t_1, t_2)$ of (T_1, T_2).

Relying on (1), the CRF can be expressed in terms of the survival copula as follows:

$$\theta(t_1, t_2) = \frac{C[S_1(t_1), S_2(t_2)]\ C^{(1,2)}[S_1(t_1), S_2(t_2)]}{C^{(1)}[S_1(t_1), S_2(t_2)]\ C^{(2)}[S_1(t_1), S_2(t_2)]}. \tag{2}$$

In Section 2.3, we introduce a new nonparametric Bernstein-based estimator for the CRF under univariate right censoring based on expression (2).

2.3 Bernstein-based estimator for the CRF

Consider a sample $(Y_{1i}, Y_{2i}, \Delta_{1i}, \Delta_{2i})$, $i = 1, \ldots, n$, from a population with population random variables $(Y_1, Y_2, \Delta_1, \Delta_2)$. Instead of relying on a direct (smooth) estimator for the bivariate survival function, we consider a nonparametric estimator for the copula function which will subsequently be smoothed on a bounded part of the $[0, 1]^2$ domain using Bernstein polynomials. An estimator for the copula function C, valid under univariate right censoring, has been proposed by Geerdens et al. (2016) and closely relates to the Lin-Ying estimator for the bivariate survival function $S(t_1, t_2)$ (Lin and Ying 1993). In this paper, we consider the following copula estimator:

$$\widehat{C}(u_1, u_2) = \frac{n^{-1} \sum_{i=1}^{n} \mathbb{I}\left[Y_{1i} > \widehat{S}_1^{-1}(u_1), Y_{2i} > \widehat{S}_2^{-1}(u_2)\right]}{\widehat{S}_C\left[\widehat{S}_1^{-1}(u_1) \vee \widehat{S}_2^{-1}(u_2)\right]}, \tag{3}$$

for $\tau_j \leq u_j \leq 1$, where $\tau_j = S_j(t_{T_j 0})$ for $j = 1, 2$ and $t_{T_j 0}$ is introduced as a truncation point satisfying $t_{T_j 0} < t_{Y_j}$. The estimators of quantile functions $S_j^{-1}(u_j) = \inf\{x : S_j(x) \leq u_j\}$ in Equation (3) are computed as $\widehat{S}_j^{-1}(u_j) = \min\{t_j : \widehat{S}_j(t_j) \leq u_j\}$, for $\tau_j \leq u_j \leq 1$ based on, for example, Kaplan–Meier estimators $\widehat{S}_j(t_j)$ for the marginal survival functions (Kaplan and Meier 1958).

The restriction through the truncation points $(t_{T_1 0}, t_{T_2 0})$ ensures that estimation is performed away from the upper boundary of the support of the marginal distributions. Such a restriction is essential in the present context, as copulas and copula densities are well known to exhibit unstable behavior near the boundaries of (the subset of) the unit square. In particular, for many commonly used copula families, the copula density estimator may become highly irregular or even diverge while approaching the boundaries. This boundary effect may be further strengthened in the presence of censoring, where the effective sample size in the tail region is limited. By restricting attention to $u_j \in [\tau_j, 1]$ for $j = 1, 2$, we aim to avoid estimation in regions where the copula and copula density are impossible to estimate consistently, thereby improving both numerical stability and ensuring reliable estimates.

When estimating the CRF, as is seen in (2), in addition to an estimator of the copula function itself, estimators for its partial derivatives and the copula density are also required. Therefore, we smooth the non-smooth estimator in (3) using Bernstein polynomials on a the domain $[\tau_1, 1] \times [\tau_2, 1] \subset [0, 1]^2$ as follows:

$$\widehat{C}_m(u_1, u_2) = \sum_{k=0}^{m} \sum_{l=0}^{m} \widehat{C}(f_k, f_l) P_{mk}(w_1) P_{ml}(w_2),$$

with arguments f_k and f_l defined as:

$$f_k = \tau_1 + (1 - \tau_1)\frac{k}{m},$$

$$f_l = \tau_2 + (1 - \tau_2)\frac{l}{m},$$

and with Bernstein polynomials of order m, for $k, l = 0, 1, \ldots, m$,

$$P_{mk}(w_1) = \binom{m}{k} w_1^k (1 - w_1)^{m-k},$$

$$P_{ml}(w_2) = \binom{m}{l} w_2^l (1 - w_2)^{m-l},$$

representing binomial probabilities evaluated in $w_j = \frac{u_j - \tau_j}{1 - \tau_j}$. Note that the Bernstein smoothing is performed on the restricted domain of the unit square at which information about the bivariate event time process is available. This is in line with earlier work in the context of Bernstein-based estimation of the bivariate CDF (Dib et al. 2021).

Our Bernstein-based estimator for the CRF therefore becomes

$$\widehat{\theta}(t_1, t_2) = \frac{\widehat{C}_m[\widehat{S}_1(t_1), \widehat{S}_2(t_2)]\ \widehat{C}_m^{(1,2)}[\widehat{S}_1(t_1), \widehat{S}_2(t_2)]}{\widehat{C}_m^{(1)}[\widehat{S}_1(t_1), \widehat{S}_2(t_2)]\ \widehat{C}_m^{(2)}[\widehat{S}_1(t_1), \widehat{S}_2(t_2)]}, \tag{4}$$

with estimators for the partial derivatives of the copula function and the copula density, representing the second order partial derivative of the copula function with regard to u_1 and u_2, given as

$$\widehat{C}_m^{(1)}(u_1, u_2) = \frac{m}{1 - \tau_1} \sum_{k=0}^{m-1} \sum_{l=0}^{m} \left\{ \widehat{C}(f_{k+1}, f_l) - \widehat{C}(f_k, f_l) \right\} P_{m-1,k}(w_1) P_{ml}(w_2),$$

$$\widehat{C}_m^{(2)}(u_1, u_2) = \frac{m}{1 - \tau_2} \sum_{k=0}^{m} \sum_{l=0}^{m-1} \left\{ \widehat{C}(f_k, f_{l+1}) - \widehat{C}(f_k, f_l) \right\} P_{mk}(w_1) P_{m-1,l}(w_2),$$

$$\begin{aligned} \widehat{C}_m^{(1,2)}(u_1, u_2) = \frac{m^2}{(1 - \tau_1)(1 - \tau_2)} \sum_{k=0}^{m-1} \sum_{l=0}^{m-1} \Big\{ & \widehat{C}(f_{k+1}, f_{l+1}) + \widehat{C}(f_k, f_l) \\ & - \widehat{C}(f_{k+1}, f_l) - \widehat{C}(f_k, f_{l+1}) \Big\} P_{m-1,k}(w_1) P_{m-1,l}(w_2). \end{aligned}$$

Remark 1: The copula estimator introduced in Equation (3) is not necessarily monotone implying that the copula estimator itself is not a (survival) copula function. For the numerical results shown in Section 3, the proposed estimator is monotonized first in order to fulfill the necessary conditions for it to be a copula function. More specifically, entire monotonicity as defined by Fang et al. (2021) is imposed through a linear programming modeling approach (using the `R` packages `lpSolve` and `limSolve`). This monotone version provides estimates of the copula function that are very close to the original estimates in the simulated data. A more extensive comparison between different algorithms to monotonize the copula estimator is considered beyond the scope of this manuscript.

Remark 2: Next to a simulation-based exploration of the finite sample behavior of our proposed Bernstein-based estimator also the large sample (asymptotic) behavior could be studied. First of all, consistency of the different components of the CRF, including the copula function and its first and second order partial derivatives need to be established. For the copula function itself, one can rely on a.s. consistency proofs in Geerdens et al. (2016) for the more general case of bivariate censoring, though an extension to Bernstein-based estimation is required. For this reason, one needs to confine attention to a restricted region of the unit square at which Bernstein smoothing is performed (see, e.g., Dib et al. 2021). Unlike the assumption made in Dib et al. (2021), the marginal survival probabilities in the upper endpoints of the support of the observation times are random, thereby complicating the consistency proofs for the proposed Bernstein-smoothed copula estimator. Similar proofs for the partial derivatives, including the copula density, are therefore equally difficult to obtain. Asymptotic i.i.d. representations – needed to establish asymptotic normality – for nonparametric Bernstein-based

estimators of the various components of the CRF should be obtained first, after which technical calculations are needed to obtain an explicit expression for the asymptotic variance of the limiting normal distribution of the CRF estimator as a whole. Note that this variance expression, based on a linearisation of the CRF and variance expressions for each of the components, will contain several unknown distributional quantities, limiting its practical use. Given the aforementioned complexities surrounding these theoretical derivations, we opted to include a simulation-based perspective on the finite sample behavior of our estimator and further theoretical work is considered future work. Moreover, as the asymptotic variance of our estimator is unavailable, from a practical point of view, we rely on the bootstrap method to estimate the variability related to our Bernstein-based estimator in both the simulations and data application.

3 Simulation study

Through an extensive simulation study, we demonstrate the finite-sample performance of our proposed Bernstein-based estimator for the CRF in (4). First, we introduce the simulation setup in Section 3.1. Second, we describe the metrics used for the evaluation of the simulation results in Section 3.2. In Section 3.3, we discuss the simulation results in detail for the Clayton copula. In Section 3.4, we summarize the results for the independence, Gumbel and Frank copula, of which the results are given in the Supplementary Material. Finally, we provide a brief discussion on results obtained from a parametric approach, described in Appendix A, in Section 3.6.

3.1 Simulation setup

We generate n pairs of realisations of (T_{1i}, T_{2i}), $i = 1, \dots, n$ using the `Copula.surv` package in R. In particular, random samples of (U_{1i}, U_{2i}), $i = 1, \dots, n$ are drawn from an underlying Archimedean copula function (i.e., independence, Clayton, Gumbel or Frank copula), as well as from the rotated Hüsler–Reiss survival copula, which is an non-Archimedean copula implying upper tail dependence. Different copula parameter values θ_C are considered implying either low, moderate or high global association expressed in terms of Kendall's tau values $\tau_K = 0.2, 0.5$ or 0.8, respectively. Weibull marginal distributions for the event times are considered with scale and shape parameters denoted by λ_j and k_j, respectively. In our simulations, we choose $\lambda_j = 1$ and $k_j = 0.5$ for $j = 1, 2$. The censoring variables C_i, $i = 1, \dots, n$ are assumed to be independent from the event times T_{1i} and T_{2i}, and are assumed to follow an exponential distribution with rate parameter λ_C, or a Weibull distribution with shape and scale parameter k_C and l_C, respectively. More specifically, we explore rates $\lambda_C = 0.38, 1.33$ or 5.7 (exponential censoring; EC), and $k_C = 0.30$, $l_C = 16, 1.46$ or 0.15 (Weibull censoring; WC), corresponding to a censoring percentage for both event times of approximately 30 %, 50 % or 70 %, respectively. In general, $R = 500$ simulation sets of sample size $n = 200$, 400 or 800 are considered for each simulation configuration. For a comprehensive overview of the different simulation settings, the reader is referred to Table 1. Needless to say, for the independence copula no copula parameter value θ_C should be chosen.

We illustrate in the main text the performance of our proposed estimator for the simulation setting with a Clayton copula, which is defined as

$$C(u_1, u_2) = \left(u_1^{-\theta_C} + u_2^{-\theta_C} - 1\right)^{-1/\theta_C},$$

with corresponding CRF $\theta(t_1, t_2) = 1 + \theta_C$, with $t_j = S_j^{-1}(u_j)$ for $j = 1, 2$ and $n = 400$, $\pi_C = 50$ % and $\tau_K = 0.5$. Furthermore, for the Clayton copula, the performance of the estimator for other sample sizes, censoring percentages and extent of global association are also discussed, but the results are provided in Section S1 of the Supplementary Material. We explore the effect of the Bernstein order by considering values $m = 5, 15$ or 25 and compare the results in terms of simulation-based bias and variance of the estimator.

Table 1: Summary of the parameter values considered in the simulations. Kendall's tau values are denoted by τ_K. Simulation configurations discussed in the main text are highlighted in bold.

Parameter	**Notation**		**Values**	
Sample size	n	200	**400**	800
Censoring percentage	π_C	30 %	**50 %**	70 %
Exponential censoring				
Censoring rate	λ_C	0.38	**1.33**	5.70
Weibull censoring				
Shape parameter	k_C	0.30	0.30	0.30
Scale parameter	l_C	16.00	1.46	0.15
Kendall's tau	τ_K	0.20	**0.50**	0.80
Copula	**Copula parameter**		**Values**	
Clayton	θ_C	0.50	**2.00**	8.00
Gumbel	θ_C	1.25	2.00	5.00
Frank	θ_C	1.86	5.74	18.19
Hüsler–Reiss	θ_C	0.51	1.35	2.56

3.2 Evaluation of performance of the Bernstein estimator

We compute an approximated version of the integrated squared error (ISE) to evaluate the performance of our CRF estimator. More specifically, for each simulation set r $(1, \dots, R)$ and a two-dimensional grid G, we evaluate:

$$\widehat{\mathrm{AISE}}_{\widehat{\theta}}^{(r)} = \sum_{(t_1,t_2)\in G} \left[\widehat{\theta}^{(r)}(t_1,t_2) - \theta(t_1,t_2)\right]^2, \tag{5}$$

where $\widehat{\theta}^{(r)}(t_1,t_2)$ is the estimator for the CRF in (t_1,t_2) based on the rth simulation set and $\theta(t_1,t_2)$ is the true CRF computed using the true copula function from which data are generated. This quantity can be used to determine the optimal Bernstein order m for a given copula and configuration (i.e., based on sample size, censoring percentage and extent of global association) which is considered, for now, out of the scope for this manuscript. $\widehat{\mathrm{AISE}}_{\widehat{\theta}}^{(r)}$-values are used to visualize estimated CRF values based on simulation sets for which the respective values fall within the 2.5 % and 97.5 % percentiles of all $\widehat{\mathrm{AISE}}_{\widehat{\theta}}^{(r)}$-values.

The two-dimensional grid G of (t_1,t_2)-values is determined as follows. For each simulation set r, we estimate τ_1 and τ_2 by taking the Kaplan-Meier estimate of the survival probability in the largest observed event time. Denote this estimate in the rth simulation as $\widehat{\tau}_j^{(r)}$ for $j = 1, 2$, and $\hat{\tau}_{jm} = \max_r \widehat{\tau}_j^{(r)}$, then $G = \left[F_1^{-1}(0.01), F_1^{-1}(1-\widehat{\tau}_{1m})\right] \times \left[F_2^{-1}(0.01), F_2^{-1}(1-\widehat{\tau}_{2m})\right]$, ranging from 0.01 to $1-\widehat{\tau}_{jm}$ in steps of size 0.01, for $j = 1, 2$.

The simulation results are summarized by means of the pointwise average of the estimates $\widehat{\theta}^{(r)}(t_1,t_2)$ across the R simulation runs, together with the empirical 2.5 % and 97.5 % percentiles. In particular, for a set $\mathcal{R}(t_1,t_2) = \left\{\widehat{\theta}^{(r)}(t_1,t_2) : r = 1, \dots, R\right\}$ representing the CRF estimates in $(t_1,t_2) \in G$ based on the R simulated datasets, we have, as the pointwise average

$$\frac{1}{R}\sum_{r=1}^{R} \widehat{\theta}^{(r)}(t_1,t_2),$$

presented together with the 2.5 % and 97.5 % percentiles of this set. As pointed out in Remark 2, no asymptotic variance for the estimator is available, hence we rely on to nonparametric bootstrap method to quantify its variance. Therefore, we assess the coverage probability of bootstrap-based 95 % confidence intervals for our nonparametric Bernstein estimator. More specifically, for the rth simulated dataset of sample size n, $B = 500$ bootstrap samples of the same size are generated by randomly sampling observations with replacement. Consequently, the nonparametric estimator is computed for each of the B bootstrap samples resulting in a set

$\mathcal{B}^{(r)}(t_1, t_2) = \left\{ \widehat{\theta}^{(b,r)}(t_1, t_2) : b = 1, \ldots, B \right\}$ for $(t_1, t_2) \in \tilde{G}$, where $\widehat{\theta}^{(b,r)}(t_1, t_2)$ represents the CRF estimator based on the bth bootstrap sample of the rth simulated dataset. The two-dimensional grid $\tilde{G}$ is defined in a similar way as G based on the maximum of the bootstrap-specific τ_j-values across all simulation runs. The pointwise coverage probability in $(t_1, t_2) \in \tilde{G}$ is defined as

$$\pi_{\text{coverage}}(t_1, t_2) = \frac{1}{R} \sum_{r=1}^{R} \mathbb{I}\left[p^{(r)}_{2.5\,\%}(t_1, t_2) < \theta(t_1, t_2) < p^{(r)}_{97.5\,\%}(t_1, t_2) \right],$$

where $p^{(r)}_{2.5\,\%}(t_1, t_2)$ and $p^{(r)}_{97.5\,\%}(t_1, t_2)$ are the 2.5 % and 97.5 % percentiles of the set of bootstrap estimates $\mathcal{B}^{(r)}(t_1, t_2)$, respectively.

3.3 Results of the Clayton copula

The results for the Clayton copula with $n = 400$, $\pi_C = 50$ % (under EC) and $\tau_K = 0.5$ are given in Figure 1. The first, second and third rows represent the results for $m = 5, 15$ and 25, respectively. In particular, in panels (a), (c) and (e), we present intersections of the estimated CRF surfaces (for varying m-values) by fixing t_1 to $F_1^{-1}(0.25)$ and changing t_2-values with $0 \leq t_2 \leq F_2^{-1}(1 - \widehat{\tau}_{2m})$. The black curve represents the pointwise average of the estimated CRF values, together with the simulation-based pointwise 95 % confidence bands (black dashed lines). Furthermore, we also show the estimated CRF values for simulation runs for which $\widehat{\text{AISE}}^{(r)}_{\widehat{\theta}}$ lies between the 2.5 % and 97.5 % percentiles of $\widehat{\text{AISE}}^{(r)}_{\widehat{\theta}}$ values across the R simulation sets (gray lines). True CRF values are depicted as red dashed lines. In panels (b), (d) and (f), we present estimated values on the main diagonal of the restricted area in the unit square, i.e., $t_1 = t_2 = F_1^{-1}(u)$ or, equivalently, $t_1 = t_2 = F_2^{-1}(u)$, with $\max(\widehat{\tau}_{1m}, \widehat{\tau}_{2m}) \leq u \leq 1$. Here $\widehat{\tau}_{1m} = 0.35$ and $\widehat{\tau}_{2m} = 0.34$.

In general, our nonparametric estimator performs well, at least for m-values which are not too small. More specifically, in panels (a) and (b), i.e. results for $m = 5$, we observe that CRF values are on average smaller than the true CRF values, while in panels (c)–(d) and (e)–(f) (for $m = 15$ and $m = 25$, respectively), the bias decreases, with some overestimation, especially for pairs with large t_1- or t_2-values. As a Clayton copula imposes upper tail dependence, more difficulties in estimating the CRF for smaller quantiles are expected, especially under $m = 5$. Furthermore, we observe that the estimator shows more uncertainty near the boundaries, which has been observed elsewhere when estimating the CRF for uncensored time-to-event data (see, e.g., Abrams et al. 2024). More specifically, for the intersections of the estimated CRF surface, we observe that the simulation-based finite-sample bias decreases as m increases, while the simulation-based variance of the estimator increases, especially near the boundaries. This implies that a trade-off between bias and variance of the estimator could be considered to identify an optimal m-value (Janssen et al. 2012, 2014, 2016). Furthermore, an improved estimate, both in terms of variance and bias, is expected when relying on local Bernstein orders $m(t_1, t_2)$ for different (t_1, t_2) pairs instead of the current global m.

The finite-sample performance of our estimator was also assessed for different sample sizes, censoring percentages and a different extent of global association (see Table 1 for specific values, and Section S1 in the Supplementary Material for the corresponding simulation results). In general, for the comparison of the performance of the estimator for different sample sizes, we refer to Figures S1 and S2. The performance improves for increasing sample size, especially in terms of variability becoming smaller. Similar results in terms of finite-sample bias are observed for different censoring percentages (Figures S3 and S4), at least for the domain G which is most restrictive in case of the largest censoring percentage. However, larger uncertainty is observed as the censoring percentage increases. Finally, the performance of the proposed CRF estimator is studied for different degrees of implied global association. The best performance is obtained for the smallest value of Kendall's tau (see Figures S5 and S6).

The pointwise coverage probabilities for the bootstrap-based confidence intervals are graphically depicted in Figure 2 for different intersections of the CRF surface and $m = 5$ (black line), $m = 15$ (blue line) and $m = 25$ (gray line). In general, the coverage probabilities increase with increasing m value. Severe under-coverage is

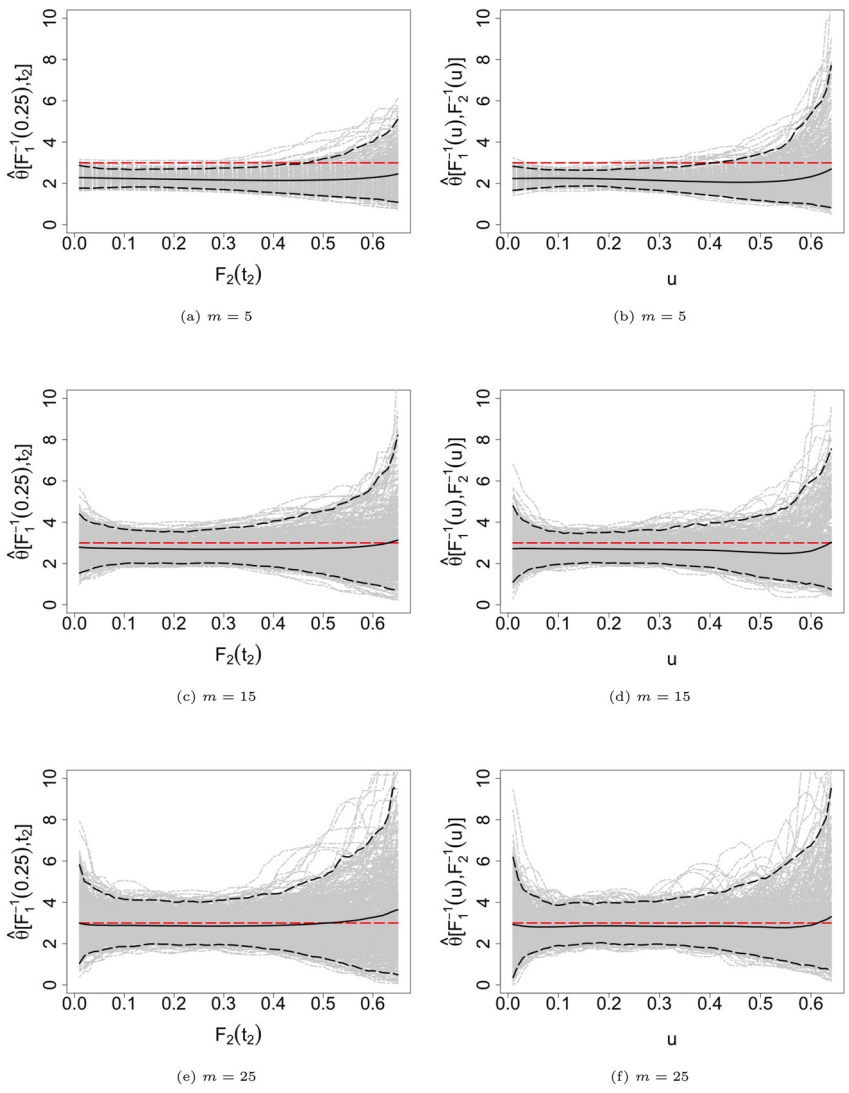

(a) $m = 5$ (b) $m = 5$

(c) $m = 15$ (d) $m = 15$

(e) $m = 25$ (f) $m = 25$

Figure 1: Clayton copula simulation setting with $m = 5$, $m = 15$, $m = 25$ (panels in first, second and third row, respectively), $n = 400$, $\pi_c = 50\,\%$ (exponential censoring) and $\tau_K = 0.5$. Panels (a), (c) and (e) present $\widehat{\theta}^{(r)}(F_1^{-1}(0.25), t_2)$ and (b), (d) and (f) depict $\widehat{\theta}^{(r)}(F_1^{-1}(u), F_2^{-1}(u))$. Black solid lines represent the pointwise averages, while the black dashed lines represent pointwise 95 % percentile-based confidence intervals for the CRF. The gray lines are the estimated CRF corresponding to $\widehat{\mathrm{AISE}}_{\hat{\theta}}^{(r)}$-values lying within the 2.5 % and 97.5 % percentiles of all $\widehat{\mathrm{AISE}}_{\hat{\theta}}^{(r)}$. The true CRF values are presented as red dashed lines.

observed for $m = 5$ while coverage probabilities are close to the nominal level of 95 % for the larger m values considered. This motivates the choice for a sufficiently large m value in order for the Bernstein estimator to perform well.

3.4 Results for other copulas

The specific results regarding the finite-sample performance of the estimator for simulations with $n = 400$, $\pi_C = 50\,\%$ and $\tau_K = 0.5$ and for the independence, Gumbel, Frank and rotated Hüsler–Reiss copulas are given in Section S2 of the Supplementary Material, however, we discuss these results briefly here.

In Figure S7, the simulation results for the independence copula are given. In general, no notable effects of different m-values are seen with regard to the bias of the estimator, however, an increase in the variability can

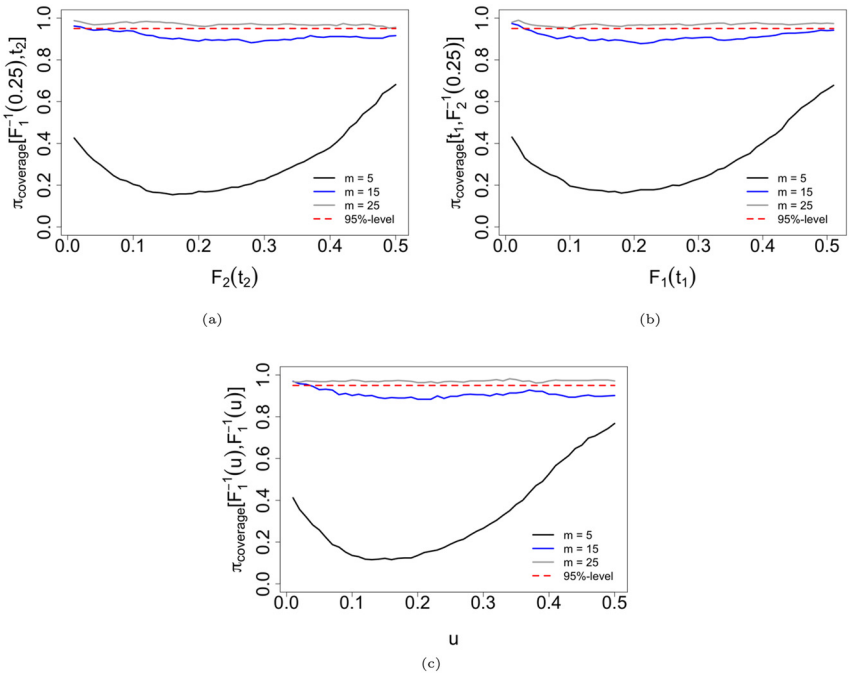

Figure 2: Pointwise coverage probabilities based on bootstrap-based confidence intervals for the Clayton copula setting with $n = 400$, $\pi_C = 50\ \%$ and $\tau_K = 0.5$ and Bernstein orders $m = 5$, $m = 15$ and $m = 25$ for the Bernstein estimator applied to each of the bootstrap samples (black, blue and gray lines, respectively). Panel (a) represents $\pi_{\text{coverage}}(F_1^{-1}(0.25), t_2)$, (b) $\pi_{\text{coverage}}(t_1, F_2^{-1}(0.25))$ and (c) $\pi_{\text{coverage}}(F_1^{-1}(u), F_2^{-1}(u))$. The red dashed line corresponds to the nominal 95 %-level.

be noted. For the Gumbel copula, an underestimation of the CRF is observed for pairs with small t_1- and t_2-values (see diagonal intersection of estimated CRF surfaces in panels (b), (d) and (f) of Figure S8). Note that the Gumbel copula gives rise to lower tail dependence. For the Frank copula (Figure S9), the performance of the estimator is worse for large t_1-values and small t_2-values, and vice versa, as the Frank copula imposes dependence around the mode of (T_1, T_2). Again, an increase in m-value leads to an improvement in terms of the bias. Similar conclusions can be drawn for the non-Archimedean rotated Hüsler–Reiss copula, imposing upper tail dependence. Difficulties in estimating the CRF for lower quantiles is observed, which is clearly shown on the main diagonal of the CRF domain where $t_1 = t_2$.

3.5 Pointwise performance of the CRF estimator across copulas

A more detailed comparison of the performance of the proposed estimator across the different copulas, for the configuration with sample size $n = 400$, censoring percentage $\pi_C = 50\ \%$, and Kendall's tau $\tau_K = 0.50$, is presented in Table 2. In particular, the estimator is evaluated at selected points of $(F_1(t_1), F_2(t_2))$ for $m = 5, 15$ and 25, for EC and WC. Pointwise performance is assessed in terms of bias, variance, and mean squared error (MSE). The bias is computed as follows

$$\frac{1}{R}\sum_{r=1}^{R}\widehat{\theta}^{(r)}(t_1, t_2) - \theta(t_1, t_2),$$

whereas the variance is estimated as the empirical variance of the set $\mathcal{R}(t_1, t_2)$. The MSE is then obtained as the sum of the squared bias and the variance. We show the performance of the estimator for $F_1(t_1) = 0.10, 0.35, 0.60$ and $F_2(t_2) = 0.10, 0.35, 0.60$. We present the MSE in Table 2, whereas in Tables S1 and S2 in the Supplementary Material, also the bias and the variance are shown, under EC and WC, respectively.

Table 2: Pointwise MSE of the CRF estimator for $n = 400$, $\pi_C = 50\ \%$ and $\tau_K = 0.5$ under exponential censoring (EC) and Weibull censoring (WC).

$(F_1(t_1), F_2(t_2))$	Copula	$m = 5$		$m = 15$		$m = 25$	
		EC	WC	EC	WC	EC	WC
(0.10, 0.10)	Independence	0.020	0.020	0.049	0.058	0.075	0.097
	Clayton	0.609	0.765	0.236	0.280	0.300	0.375
	Gumbel	21.374	19.086	8.063	2.817	4.898	1.929
	Frank	4.303	5.292	1.183	1.547	0.827	1.173
	Hüsler–Reiss	0.454	0.621	0.156	0.222	0.230	0.332
(0.10, 0.35)	Independence	0.031	0.016	0.074	0.058	0.119	0.101
	Clayton	0.669	0.911	0.364	0.317	0.575	0.438
	Gumbel	0.853	0.342	0.506	1.954	0.907	5.437
	Frank	1.660	2.255	0.655	0.712	0.904	0.797
	Hüsler–Reiss	0.230	0.296	0.226	0.198	0.360	0.336
(0.10, 0.60)	Independence	0.197	0.016	0.506	0.077	0.930	0.135
	Clayton	0.929	1.178	2.281	0.555	5.077	1.062
	Gumbel	0.522	0.089	2.435	3.114	6.358	9.209
	Frank	0.622	0.433	2.733	0.617	5.941	1.720
	Hüsler–Reiss	0.568	0.361	1.454	0.273	3.041	0.567
(0.35, 0.35)	Independence	0.023	0.007	0.046	0.031	0.080	0.057
	Clayton	0.912	1.245	0.333	0.350	0.398	0.308
	Gumbel	2.054	1.529	1.055	0.242	0.882	0.392
	Frank	2.977	3.596	1.299	1.563	1.031	1.099
	Hüsler–Reiss	0.419	0.490	0.245	0.242	0.277	0.251
(0.60, 0.35)	Independence	0.111	0.006	0.263	0.036	0.480	0.077
	Clayton	1.184	1.707	1.173	0.534	2.153	0.502
	Gumbel	1.153	0.921	1.130	0.216	1.598	0.406
	Frank	2.320	2.957	1.888	1.539	2.377	1.221
	Hüsler–Reiss	0.485	0.334	0.878	0.160	1.596	0.226
(0.60, 0.60)	Independence	0.208	0.005	0.533	0.029	2.445	0.061
	Clayton	2.503	2.347	4.003	0.757	7.552	0.515
	Gumbel	0.840	0.336	1.165	0.079	2.220	0.218
	Frank	1.454	1.233	1.465	0.644	1.641	0.515
	Hüsler–Reiss	1.978	0.411	1.504	0.146	2.787	0.187

For the independence copula, we observe that, for all points $(F_1(t_1), F_2(t_2))$, the MSE increases with increasing m, irrespective of the censoring process imposed. As shown in Table 2, this behavior is driven by a negligible bias, while the variance increases with increasing m, thereby inducing the monotonic growth of MSE. In contrast, for the Clayton, Gumbel, Frank, and rotated Hüsler–Reiss copulas, a clear trade-off between the squared bias and the variance is observed. Consequently, for most evaluation points, the MSE at $m = 15$ is smallest, providing a convex shape of MSE in relation to m underlining the interplay between bias and variance. See also Tables S1 and S2 in the Supplementary Material.

Another important aspect concerns the behavior of our Bernstein-based estimator near the upper endpoint of the predefined domain. In particular, for the Clayton and rotated Hüsler–Reiss copulas, which exhibit upper tail dependence between event times, a substantial decline in performance is observed under EC compared to WC. This is explained by the fact that the tail of the censoring distribution is heavier under WC compared to EC in relation to the tail of the marginal event time distributions. Specifically, the exponentially distributed censoring times tend to limit the observation of event times in the upper tail, whereas the Weibull censoring distribution allows for more observations in the upper right region of the (T_1, T_2)-domain. We refer to Figure 3 for a depiction of the probability density functions for the different distributions with the black line showing the

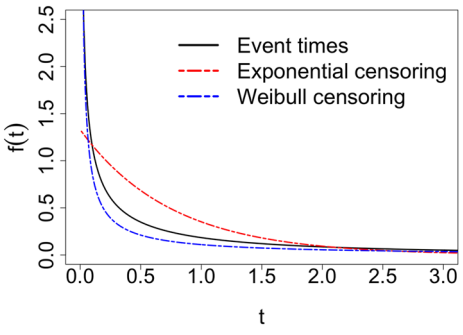

Figure 3: Density functions of the event times and censoring times. In particular, black line shows the density function of a Weibull distribution with shape and scale parameters $k_j = 0.5$ and $\lambda_j = 1$, respectively, for $j = 1, 2$. On the other hand, the red dashed line shows the density of an exponential distribution with rate parameter $\lambda_C = 1.33$, whereas the blue dashed line represents the density function of a Weibull distribution with shape and scale parameter $k_C = 0.3$ and $l_C = 1.46$, respectively. Both impose a censoring rate of 50 % on both the event times.

density function for the event times. Moreover, the red dashed line shows the density function of the exponential censoring distribution with $\lambda_C = 1.33$, while the blue dashed line represents the density of the Weibull censoring distribution with $k_C = 0.3$ and $l_C = 1.46$, both imposing a censoring percentage of 50 % in both event times.

3.6 Results of parametric approach

Finally, parametric CRF estimation is considered as an alternative to nonparametric Bernstein-based estimation. Attention is restricted here to the Clayton, Gumbel and Frank copulas. Details with respect to estimation for these parametric CRF estimators are provided in Appendix A. In this subsection, we give a brief overview of the key results with regard to the comparison of these estimators. As expected, parametric estimators for the CRF are unbiased and exhibit smaller empirical standard errors across the different settings as compared to the nonparametric counterparts, at least while relying on a correctly specified parametric model for both the marginal distributions as well as the association structure (i.e., copula function).

For increasing sample sizes (see, e.g., Figures A1–A3 in Appendix A.1 for the Clayton copula setting), finite sample bias and simulation-based variance and bias decrease. Moreover, the simulation-based variance increases with increasing censoring percentages (Figures A2, A4 and A5 for $\pi_C = 30$ %, $\pi_C = 50$ %, and $\pi_C = 70$ %, respectively) and stronger global association (Figures A2, A6 and A7 for $\tau_K = 0.2$, $\tau_K = 0.5$, and $\tau_K = 0.8$, respectively). For illustrative purposes and completeness, parametric CRF estimation under Frank and Gumbel copula association are shown in Appendix A.2 (Figures A8 and A9) with similar conclusions.

Although parametric estimators show excellent performance under a correctly specified model, in practice, parametric assumptions can be violated. Our proposed nonparametric estimator, however, requires neither the selection of a parametric family for the marginal distributions nor the specification of a particular association structure through a bivariate copula function. The Bernstein-based nonparametric estimator for the CRF has good coverage results for sufficiently large m-values, whereas parametric estimators demonstrate severe undercoverage when the model is misspecified (see Figure A10 in Appendix A.3).

4 Data application

A real-life data application is used to demonstrate the use of the proposed Bernstein-based CRF estimator. The dataset under study is well-known and contains information about patients at high risk of developing diabetic retinopathy. This dataset has been considered for analysis by Huster et al. (1989) and Geerdens et al. (2017), among others. Diabetic retinopathy is a medical condition in which the retina (light sensitive layer of tissue at the back of the eyeball) is damaged as a result of diabetes mellitus. Data on $n = 197$ patients was available for which either the left or the right eye was treated using a Xenon ($n_1 = 100$) or Argon laser ($n_2 = 97$). The other eye of each patient remained untreated. The dataset is available in R through the `survival` package.

The event times of interest are the time between treatment (in one of the two eyes) and the drop in visual acuity below 5/200 in two consecutive visits, measured in treated (denoted by T_1) and untreated eyes (i.e., T_2). The event times in the dataset are actually the event time of interest (i.e., the time between treatment and the second visit after treatment) minus 6.5 months. Univariate right censoring was caused by death, dropout, or end of study period (administrative censoring) for both eyes simultaneously.

4.1 Data exploration

In Figure 4, we present a scatter plot of the data with dots representing subjects for which both events are observed, triangles imply right censoring of one of the two event times, and crosses refer to univariate right censoring of both events. As seen in this figure, the percentage of censoring is high with 72.6 % and 48.7 % of all observations being right-censored for the first and second event time, respectively.

4.2 Estimation of the CRF

In this data application, we demonstrate the practical performance of our nonparametric CRF estimator. Based on the coverage results presented in Section 3.3, we choose $m = 20$, thereby avoiding biased estimation of the CRF. First, we study local association based on the estimated CRF for all bivariate event time data together.

Figure 5 shows the results of estimating the CRF using the novel nonparametric Bernstein-based estimator. In panel (a), a heatmap of the estimated CRF values is presented. Panels (b), (c) and (d) depict the estimated CRF values $\widehat{\theta}(t_1, t_2)$ when fixing t_2-values to the 25 %, 50 % and 75 % quartiles, respectively, of the observed event times, and varying t_1-values. More specifically, results are based on $B = 500$ nonparametric bootstrap samples obtained by resampling with replacement from the original sample. The black solid line represents the pointwise median of the B bootstrap-based estimates for the cross ratio function values in (t_1, t_2), together with pointwise bootstrap-based 95 % confidence intervals (depicted in blue). We confine attention to the domain defined by τ_1 as pointed out in Section 3, with the most restrictive value considered across different bootstrap runs. In general, CRF values are found to differ from one between 13.5 and 32.5 months after treatment (i.e. between $t_1 = 7$ and $t_1 = 26$), at least when conditioning on blindness for the untreated eye at 13.5 months after treatment ($t_2 = 7$, the first quartile of the observed event times in the untreated eyes). This implies that the hazard of blindness (visual acuity below the aforementioned threshold) for the treated eye between 13.5 and 32.5 months after treatment is estimated to be higher among those individuals experiencing visual loss in the untreated eye at 13.5 months after treatment compared to individuals for which blindness was not yet observed in the untreated eye. More specifically, the hazard ratio of blindness is estimated to be highest around 19.5 months after treatment ($t_1 = 13$), with the hazard of blindness in the treated eye being approximately 5 times higher among those suffering from blindness in the untreated eye after 13.5 months (after treatment) as compared to those patients with loss of visual acuity below the pre-specified threshold at that time. Although the local association is estimated to be positive even for higher t_2-values, the uncertainty is large. Stated differently, for those patients that experience blindness of the untreated eye relatively late (i.e., having large t_2-values), the hazard of visual loss in the treated

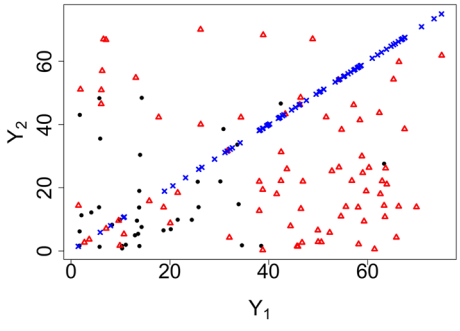

Figure 4: Scatter plot of the diabetic retinopathy data. Dots refer to subjects for which both events are observed. Red triangles refer to subjects for which one of the event times is right-censored and blue crosses to subjects for which both event times are right-censored.

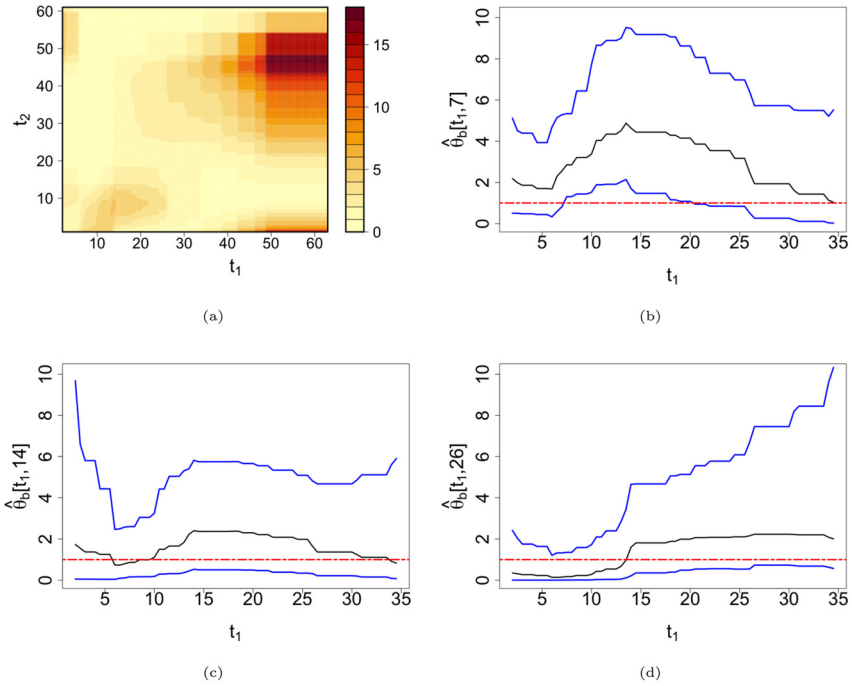

Figure 5: Estimated CRF for diabetic retinopathy data. Panel (a) represents estimated CRF surface. In panel (b), (c) and (d), we fix t_2 to the 25 %, 50 % and 75 % quartiles, respectively, of the observed event times (i.e., 7, 14 and 26 months, respectively) and vary t_1. $B = 500$ bootstrap samples are taken to compute the pointwise median (black lines) and 95 % bootstrap-based confidence intervals (blue lines). The red dashed line represents the line corresponding to no association.

eye is not different from the risk in those patients suffering from blindness beyond the specific time point that is considered.

4.3 Differences between treatment groups

Next, differences between Argon or Xenon laser treatment are examined. Figures 6 and S11 in the Supplementary Material present CRF values for these groups, including a relative comparison of CRF values between treatments. In particular, the subset of patients receiving Xenon and Argon laser treatment are nonparametrically resampled $B = 500$ times and the corresponding CRF values are estimated for varying t_1-values while fixing t_2 to the 25 % (Figure 6), 50 % or 75 % (i.e., $t_2 = 7$, $t_2 = 14$ and $t_2 = 26$, respectively) quartiles of the observed Y_2 values (Figure S11). We compute the pointwise median (black line) and bootstrap-based 95 % confidence intervals (blue lines).

At 13.5 months after treatment ($t_2 = 7$), a higher local association is observed among patients receiving Xenon laser treatment. The difference becomes larger after 19.5 months after treatment ($t_1 = 13$), as is clear from panel (c) in Figure 6. This suggests that, for patients with Xenon treatment, the hazard of visual loss for the treated eye (especially later than 19.5 months after treatment) is estimated to be higher among those having visual loss in the untreated eye at time 13.5 months after treatment ($t_2 = 7$), as compared to those for which blindness was not observed yet in the untreated eye. This instantaneous risk is observed to be lower among patients under Argon laser treatment. However, as we switch to $t_2 = 14$ and $t_2 = 26$ (20.5 and 32.5 months after treatment, respectively), i.e., panels (a), (b), (c) and (d), (e), (f), respectively, of Figure S11, we note that this difference in hazard rates decreases. In general, due to the limited sample size in each of the treatment groups, the observed differences in local association are not significant.

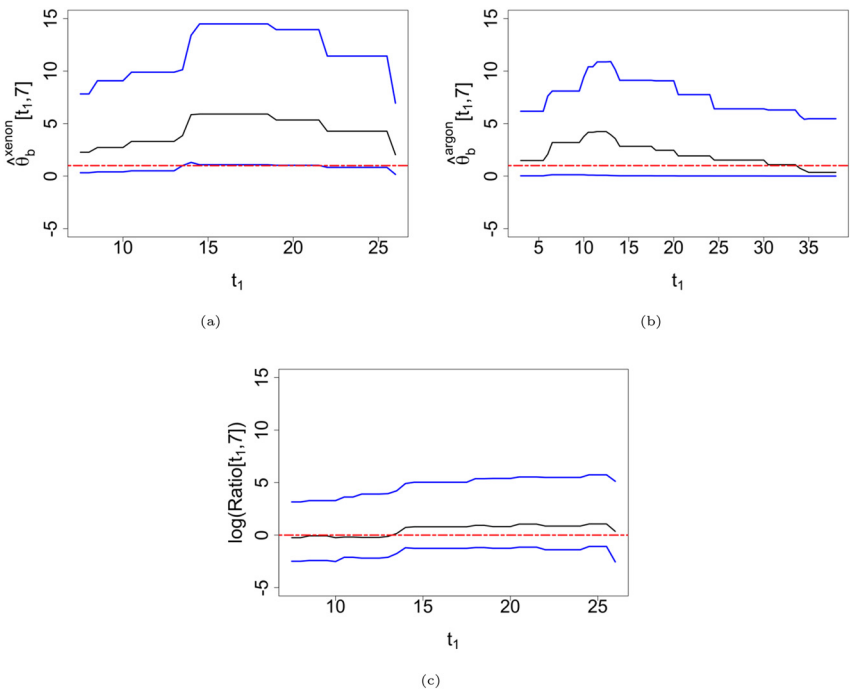

Figure 6: Estimated CRF for patients receiving Xenon and Argon laser treatment. In particular, panels (a) and (b) provide the estimated CRF values for patients receiving the Xenon laser treatment and Argon laser treatment, respectively, where t_2 is fixed to the 25 % quartile of the observed Y_2. Panel (c) represents the logarithm of the ratio of these estimated CRFs for Xenon and Argon subgroups. In all panels, for the range of t_1, most restricted domain of the B bootstraps is taken.

In panels (a) and (d) of Figure S11, we observe that the strength of the jump around 19.5 months after treatment ($t_1 = 13$) has decreased. Furthermore, in panels (b) and (e) of Figure S11, CRF values are close to one, implying a decrease of local association among patients receiving Argon treatment. Panels (c) and (f) confirm the decrease of the risk difference, as the logarithm of the ratio of the CRFs also approximates the zero-line. For the optimal treatment, we expect the association to be lowest (i.e., smallest CRF values), however, no strong evidence for such a difference is found. Although treatment effect are found to be strongest for $t_2 = 26$ (i.e., 32.5 months after treatment) for both Xenon and Argon laser treatment (panels (d) and (e) of Figure S11), the effects do not seem to be very different (see panel (f) in Figure S11).

In earlier analyses conducted by Huster et al. (1989) and Geerdens et al. (2017), the impact of age at diabetes and treatment on the outcome of interest was studied. We investigated how different treatments (i.e. Xenon and Argon laser treatment) impact the association between loss of visual acuity for treated and untreated eyes. Our results are in line with the work conducted by Plumb et al. (1982) in which Xenon laser photocoagulation was found to have a higher effectiveness in delaying the onset of blindness in diabetic retinopathy patients, albeit non-significant. In particular, the quarterly evolution of visual acuity in Argon treatment group and Xenon treatment group were compared. The evolution in the Xenon treatment group showed a better course than the evolution under Argon treatment, however, the lack of statistical significance made the difference in the course not worthy. Studying the use of the CRF and given the chosen Bernstein order, a more granular view on local association allows for a more detailed investigation of whether and when differences between treatments exist. Consequently, additional information on whether and when Xenon (and Argon) treatment lowers the risk of blindness among patients is provided. In general, the CRF provides local information about specific regions of the bivariate time (to blindness) domain in which treatment effects and differences are most pronounced.

5 Discussion

In this paper, we proposed a novel Bernstein-based nonparametric estimator for the cross ratio function, which is applicable to univariate right-censored time-to-event data. The primary focus in this paper was on the assessment of the finite-sample performance of the novel estimator through an extensive simulation study and on its applicability to a real-life data application. In general, simulation results show a good finite-sample performance in terms of simulation-based finite-sample bias and variance. In general, larger sample sizes implied smaller bias and decreasing variability which provides simulation-based evidence of consistency. Increasing levels of censoring induced lower precision.

Despite the limited sample size of the data application at hand, the estimator provides valuable insights into the local association of the bivariate time-to-event outcomes. For this analysis, we selected a Bernstein order of $m = 20$ to reduce bias, accepting increase in variability while aiming to avoid undercoverage of the bootstrap-based confidence intervals. A comparison with the parametric approaches is provided in the appendix. Based on the simulation results, we observed that increasing m decreases bias but introduces additional noise into the estimator and improves coverage; however, further increases in m eventually lead to overcoverage. Accordingly, we selected $m = 20$ as an appropriate balance between the trade of bias and variability and coverage.

A theoretical investigation of the properties of the novel nonparametric estimator is currently lacking and not part of this study. A theoretical investigation in the context of Bernstein-based copula estimation was performed by Dib et al. (2021) for the case of one-component right censoring (e.g., uniform consistency), though thereby confining attention to a fixed endpoint τ_1. However, for the estimation of the CRF under univariate right censoring, Kaplan–Meier estimators for the marginal survival functions are involved, leading to the estimation of τ_1 and τ_2, and therefore the restriction to a random bivariate square on which our proposed estimator is considered. Establishing theoretical results has its challenges as endpoints τ_1 and τ_2 are estimated and cannot be considered fixed. In earlier work of Janssen et al. (2012, 2014, 2016), a theoretical study on the Bernstein-based copula estimation was performed for uncensored time-to-event data. Furthermore, Abrams et al. (2020, 2022, 2024) provide theoretical asymptotic results on the Bernstein-based estimators for the CRF and a risk ratio as alternative quantity expressing local association, in a setting without censoring. As these methods were developed and investigated for uncensored data, they do not require estimation of such support endpoints. The latter complicates the establishment of theoretical results concerning our proposed estimator.

Although asymptotic results (such as consistency or asymptotic normality) are lacking to date, simulation-based consistency was demonstrated. Needless to say, the Bernstein order m impacts the performance of our estimator, as it has an effect on bias and variance, and an optimal choice of m depends on sample size, censoring percentage and extent of global association. Data-driven procedure to select the Bernstein order is considered an important topic for future research. A further step, as such, in the data application is redoing the analysis with the optimal Bernstein order. In particular, such an analysis performed with the optimal Bernstein order can give new insights into the (local) association of the event times, and in case of this example, more insight into the treatment effect and eventually differences in the applied treatments (Xenon and Argon laser treatment).

Other avenues for future research include an extension of the Bernstein-based estimator from univariate right-censored data to other censoring mechanisms such as one-component right censoring and bivariate right censoring (i.e., implying two censoring variables C_1 and C_2, for T_1 and T_2, respectively). This will lead to the use of other estimators of the survival copula, including other estimators of the survival function(s) of the censoring variable(s) as well (e.g. the estimator defined in Dabrowska (1988) in case of a general form of censoring mechanism). As such, adapted versions for the Bernstein-based estimator of the copula will emerge. Based on an initial simulation-based exploration, considering a more general CRF estimator including the Dabrowska estimator (Dabrowska 1988) for the bivariate survival function of the censoring variables leads to a less efficient estimation under univariate censoring (results not shown here). A more in-depth study of alternative estimators is considered beyond the scope of this manuscript.

Acknowledgments: The authors gratefully acknowledge the support of the Research Foundation-Flanders (FWO) (grant number G011022N). Furthermore, the resources and services used in this work were provided by the VSC (Flemish Supercomputer Center), funded by the Research Foundation-Flanders (FWO) and the Flemish Government. We also express our gratitude to Paul Janssen and Noël Veraverbeke for their insightful feedback. The authors thank the anonymous reviewers for their insightful comments and suggestions, which helped to improve the quality of this manuscript.
Research ethics: Not applicable.
Informed consent: Not applicable.
Author contributions: AV and SA conceived and supervised the research. OS conducted the research, implemented the proposed Bernstein-based estimator and carried out the simulation study. The data analysis was performed by OS and all authors contributed to the interpretation of the simulation and empirical results. OS prepared the manuscript, with feedback and revisions provided by AV and SA. All authors reviewed and approved the final manuscript.
Use of Large Language Models, AI and Machine Learning Tools: None declared.
Conflict of interest: The author states no conflict of interest.
Research funding: Research Foundation Flanders – FWO, Grant number G011022N.
Data availability: Not applicable.

Appendix A: Parametric estimation of the CRF

In this appendix, we demonstrate the use of parametric estimators for the CRF and compare those with the nonparametric Bernstein estimator under univariate censoring as detailed in Section 2. More specifically, direct maximum likelihood (ML) estimation for a fully parametric approach in which both the copula function (and implied association structure) as well as the marginal event time distributions are modeled parametrically is considered.

In case of no model misspecification, Weibull marginal distributions for the event times are assumed. ML estimation of the parameters associated with the marginal Weibull distributions as well as the copula parameter can be done jointly by maximizing the following likelihood function for bivariate right-censored time-to-event data with independent and non-informative censoring (Sun 2006)

$$L(\boldsymbol{\xi}) = \prod_{i=1}^{n} \left[S(Y_{1i}, Y_{2i}; \boldsymbol{\xi})\right]^{(1-\Delta_{1i})(1-\Delta_{2i})} \left[f(Y_{1i}, Y_{2i}; \boldsymbol{\xi})\right]^{\Delta_{1i}\Delta_{2i}} \cdot \left[-S^{(1)}(Y_{1i}, Y_{2i}; \boldsymbol{\xi})\right]^{\Delta_{1i}(1-\Delta_{2i})} \left[-S^{(2)}(Y_{1i}, Y_{2i}; \boldsymbol{\xi})\right]^{(1-\Delta_{1i})\Delta_{2i}},$$

where $\boldsymbol{\xi} = (\theta_C, \lambda_1, \lambda_2, k_1, k_2)$. In order to maximize the likelihood function, we rely on the `optim` function in `R`.

A.1 Clayton copula

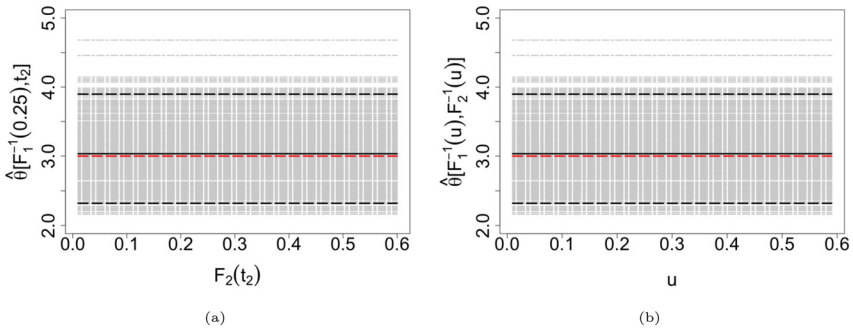

(a) (b)

Figure A1: Clayton copula simulation setting with $n = 200$, $\pi_C = 50$ % (exponential censoring) and $\tau_K = 0.5$. Panel (a) shows $\widehat{\theta}^{(r)}(t_1, F_2^{-1}(0.25))$ and panel (b) depict $\widehat{\theta}^{(r)}(F_1^{-1}(u), F_2^{-1}(u))$. Black solid lines represent the pointwise averages, while blue lines represent pointwise 95 % percentile-based confidence intervals for the CRF. Individual estimated CRF values are given in gray dashed lines. The true CRF value is presented as a red dashed line.

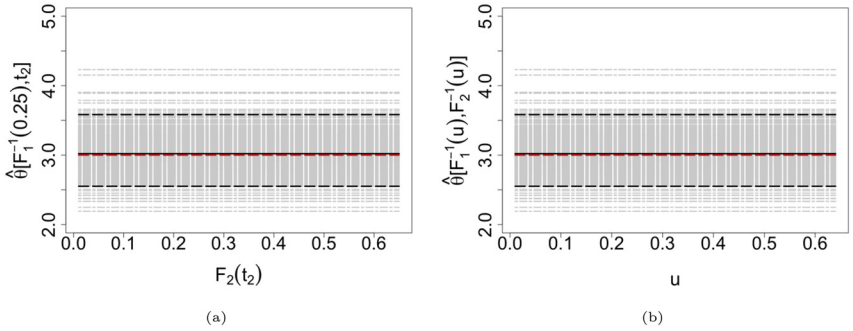

(a) (b)

Figure A2: Clayton copula simulation setting with $n = 400$, $\pi_C = 50$ % (exponential censoring) and $\tau_K = 0.5$. Panel (a) shows $\widehat{\theta}^{(r)}(t_1, F_2^{-1}(0.25))$ and panel (b) depict $\widehat{\theta}^{(r)}(F_1^{-1}(u), F_2^{-1}(u))$. Black solid lines represent the pointwise averages, while blue lines represent pointwise 95 % percentile-based confidence intervals for the CRF. Individual estimated CRF values are given in gray dashed lines. The true CRF value is presented as a red dashed line.

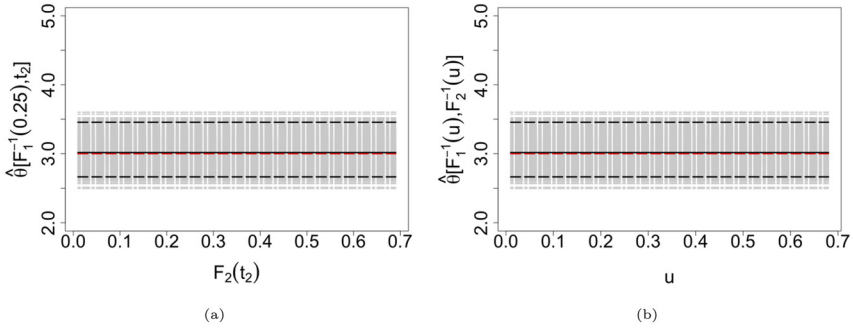

(a) (b)

Figure A3: Clayton copula simulation setting with $n = 800$, $\pi_C = 50$ % (exponential censoring) and $\tau_K = 0.5$. Panel (a) shows $\widehat{\theta}^{(r)}(t_1, F_2^{-1}(0.25))$ and panel (b) depict $\widehat{\theta}^{(r)}(F_1^{-1}(u), F_2^{-1}(u))$. Black solid lines represent the pointwise averages, while blue lines represent pointwise 95 % percentile-based confidence intervals for the CRF. Individual estimated CRF values are given in gray dashed lines. The true CRF value is presented as a red dashed line.

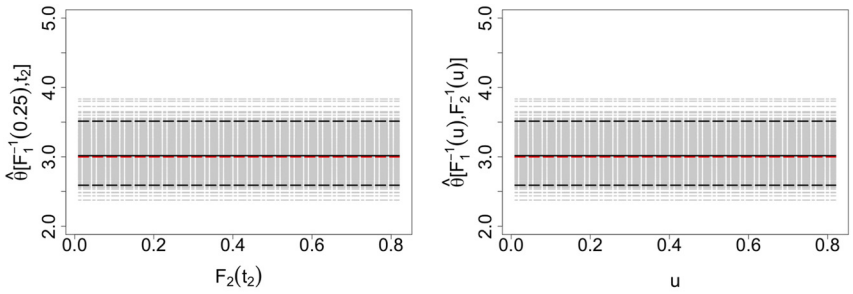

(a) (b)

Figure A4: Clayton copula simulation setting with $n = 400$, $\pi_C = 30\ \%$ (exponential censoring) and $\tau_K = 0.5$. Panel (a) shows $\widehat{\theta}^{(r)}(t_1, F_2^{-1}(0.25))$ and panel (b) depict $\widehat{\theta}^{(r)}(F_1^{-1}(u), F_2^{-1}(u))$. Black solid lines represent the pointwise averages, while blue lines represent pointwise 95 % percentile-based confidence intervals for the CRF. Individual estimated CRF values are given in gray dashed lines. The true CRF value is presented as a red dashed line.

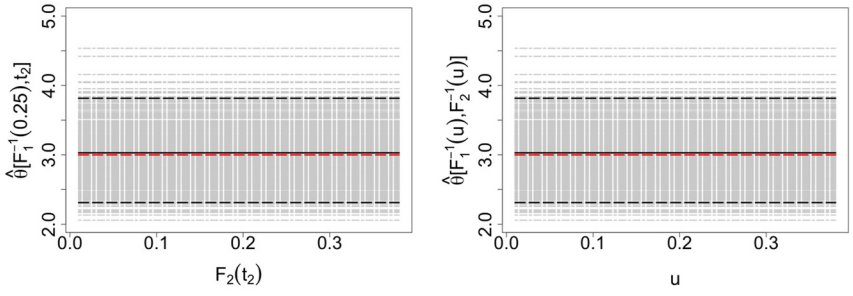

(a) (b)

Figure A5: Clayton copula simulation setting with $n = 400$, $\pi_C = 70\ \%$ (exponential censoring) and $\tau_K = 0.5$. Panel (a) shows $\widehat{\theta}^{(r)}(t_1, F_2^{-1}(0.25))$ and panel (b) depict $\widehat{\theta}^{(r)}(F_1^{-1}(u), F_2^{-1}(u))$. Black solid lines represent the pointwise averages, while blue lines represent pointwise 95 % percentile-based confidence intervals for the CRF. Individual estimated CRF values are given in gray dashed lines. The true CRF value is presented as a red dashed line.

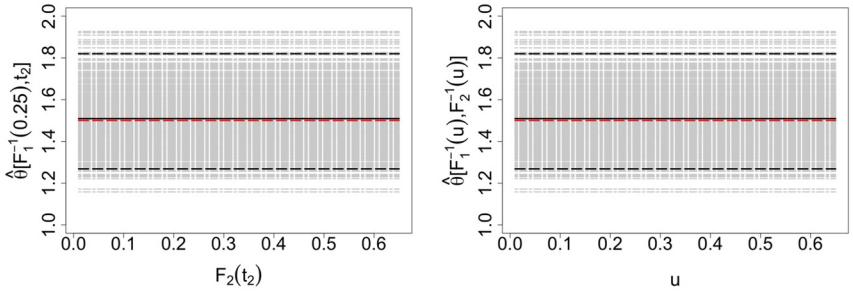

(a) (b)

Figure A6: Clayton copula simulation setting with $n = 400$, $\pi_C = 50\ \%$ (exponential censoring) and $\tau_K = 0.2$. Panel (a) shows $\widehat{\theta}^{(r)}(t_1, F_2^{-1}(0.25))$ and panel (b) depict $\widehat{\theta}^{(r)}(F_1^{-1}(u), F_2^{-1}(u))$. Black solid lines represent the pointwise averages, while blue lines represent pointwise 95 % percentile-based confidence intervals for the CRF. Individual estimated CRF values are given in gray dashed lines. The true CRF value is presented as a red dashed line.

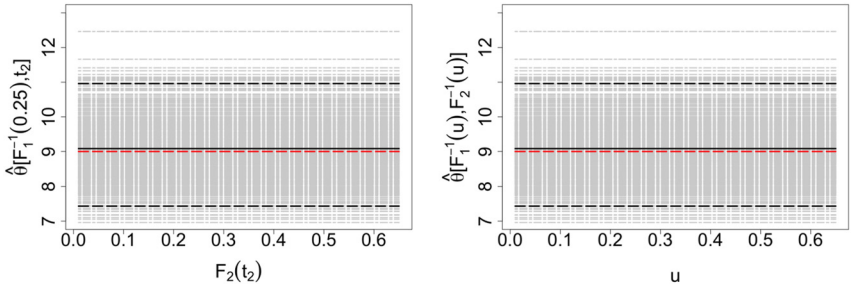

(a) (b)

Figure A7: Clayton copula simulation setting with $n = 400$, $\pi_C = 50\ \%$ (exponential censoring) and $\tau_K = 0.8$. Panel (a) shows $\widehat{\theta}^{(r)}(t_1, F_2^{-1}(0.25))$ and panel (b) depict $\widehat{\theta}^{(r)}(F_1^{-1}(u), F_2^{-1}(u))$. Black solid lines represent the pointwise averages, while blue lines represent pointwise 95 % percentile-based confidence intervals for the CRF. Individual estimated CRF values are given in gray dashed lines. The true CRF value is presented as a red dashed line.

A.2 Other copulas

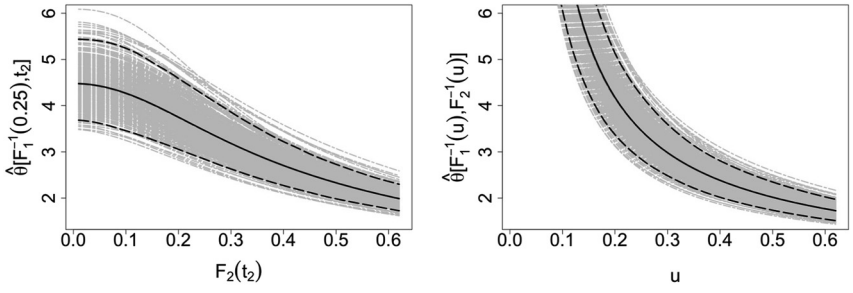

(a) (b)

Figure A8: Gumbel copula simulation setting with $n = 400$, $\pi_C = 50\ \%$ (exponential censoring) and $\tau_K = 0.5$. Panel (a) shows $\widehat{\theta}^{(r)}(t_1, F_2^{-1}(0.25))$ and panel (b) depict $\widehat{\theta}^{(r)}(F_1^{-1}(u), F_2^{-1}(u))$. Black solid lines represent the pointwise averages, while blue lines represent pointwise 95 % percentile-based confidence intervals for the CRF. Individual estimated CRF values are given in gray dashed lines. The true CRF value is presented as a red dashed line.

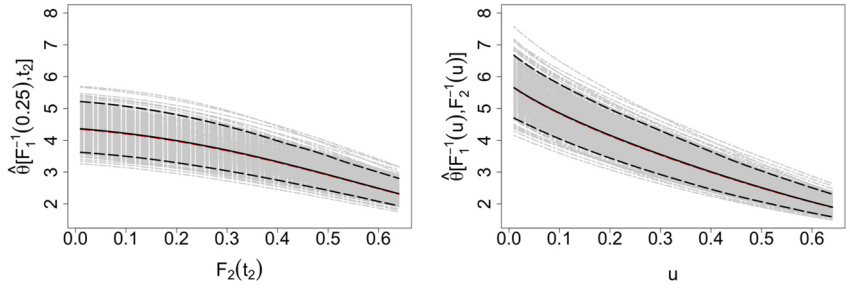

(a) (b)

Figure A9: Frank copula simulation setting with $n = 400$, $\pi_C = 50\ \%$ (exponential censoring) and $\tau_K = 0.5$. Panel (a) shows $\widehat{\theta}^{(r)}(t_1, F_2^{-1}(0.25))$ and panel (b) depict $\widehat{\theta}^{(r)}(F_1^{-1}(u), F_2^{-1}(u))$. Black solid lines represent the pointwise averages, while blue lines represent pointwise 95 % percentile-based confidence intervals for the CRF. Individual estimated CRF values are given in gray dashed lines. The true CRF value is presented as a red dashed line.

A.3 Coverage probabilities under model misspecification

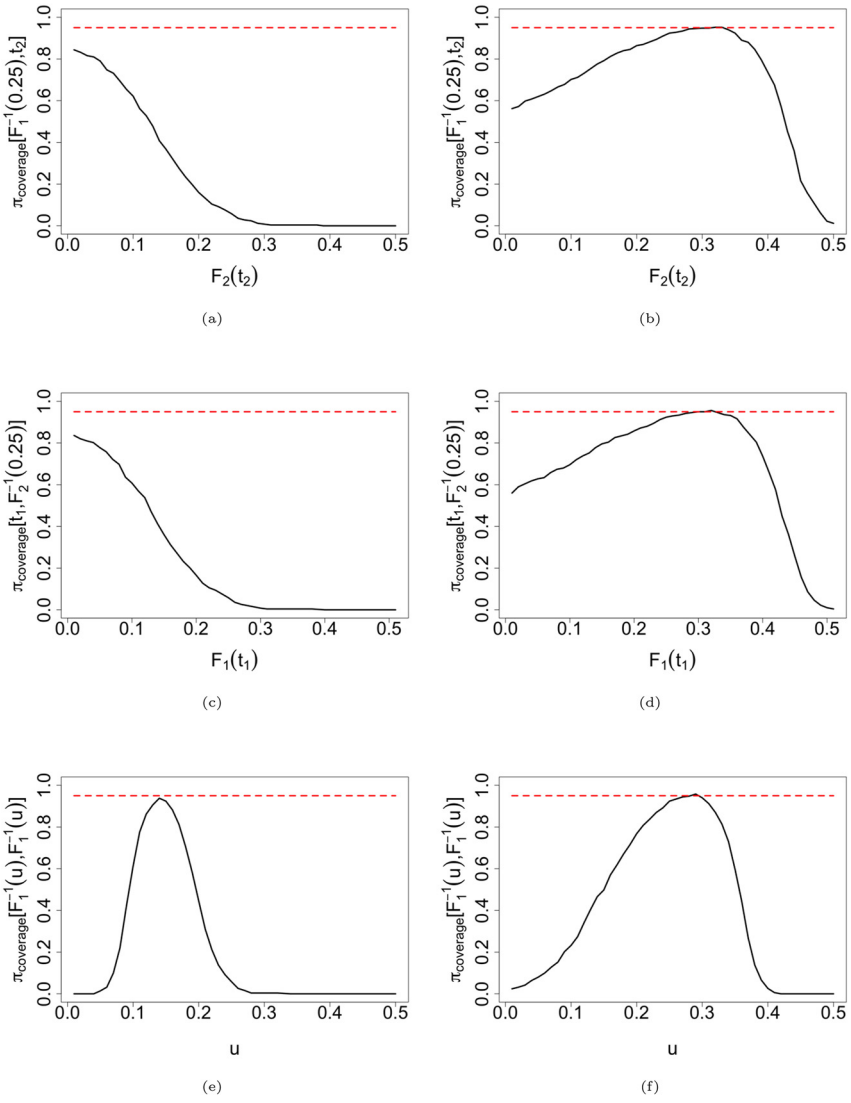

Figure A10: Pointwise coverage probabilities based on bootstrap-based confidence intervals for the Clayton copula setting with $n = 400$, $\pi_C = 50\ \%$ and $\tau_K = 0.5$ under model misspecification. First column represents the results of Gumbel assumption and second column shows the results under Frank assumption. Panels (a) and (b) represent $\pi_{\text{coverage}}(F_1^{-1}(0.25), t_2)$, (c) and (d) $\pi_{\text{coverage}}(t_1, F_2^{-1}(0.25))$ and (e) and (f) $\pi_{\text{coverage}}(F_1^{-1}(u), F_2^{-1}(u))$. The red dashed line corresponds to the nominal 95 %-level.

A.4 Data application

Parametric models were fitted to the diabetic retinopathy data introduced in Section 4. Figure A11 presents a comparison of the estimated CRF obtained from the proposed non-parametric estimator for $m = 5$, $m = 15$, and $m = 25$ in panels (a), (c), and (e), respectively. For reference, panels (b), (d), and (f) display the corresponding parametric estimates under the Clayton, Gumbel, and Frank copula models, assuming Weibull marginal distributions.

To quantify uncertainty, $B = 500$ bootstrap samples were drawn with replacement from the original dataset. The comparison is shown for $t_2 = 14$, with t_1 ranging from 0 to 35, corresponding to the most restricted domain

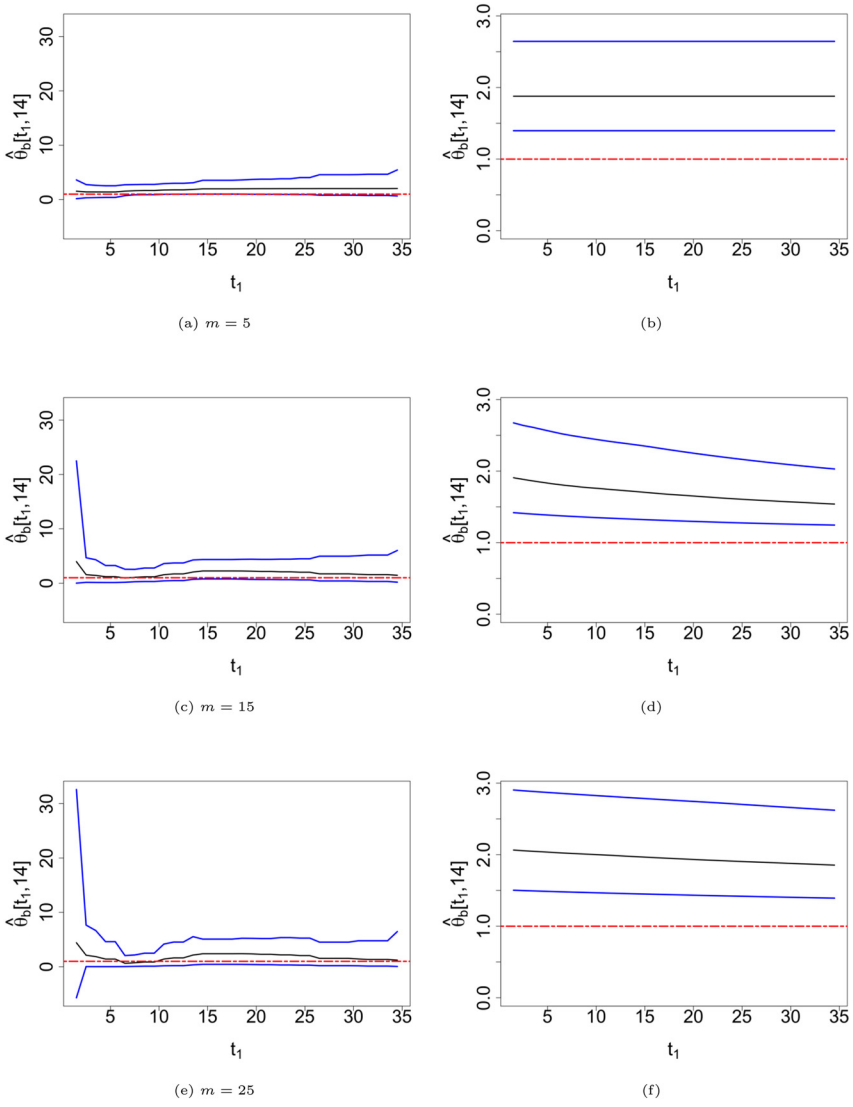

Figure A11: Estimated CRF on the retinopathy data. Panels (a), (c) and (e) correspond with the proposed non-parametric estimator with Bernstein order $m = 5$, $m = 15$ and $m = 25$, respectively. Panels (b), (d) and (f) display the parametric approach under Clayton, Gumbel and Frank assumptions, respectively, with Weibull distribution assumption for the marginals. Comparison is shown for the most restricted area across the bootstrap samples. Black lines correspond with the pointwise average across the bootstrap estimated and the blue lines show the 95 % bootstrap-based uncertainty. The red dashed line corresponds with no association.

of available data (as discussed previously). The black curves represent the pointwise bootstrap means, while the blue curves denote the associated 95 % bootstrap-based confidence intervals. The dashed red line indicates the line of no association.

References

Abrams, S., Janssen, P., Swanepoel, J., and Veraverbeke, N. (2020). Nonparametric estimation of the cross ratio function. *Ann. Inst. Stat. Math.* 72: 771–801.

Abrams, S., Janssen, P., Swanepoel, J., and Veraverbeke, N. (2022). Nonparametric estimation of risk ratios for bivariate data. *J. Nonparametric Stat.* 34: 940–963.

Abrams, S., Sercik, O., and Veraverbeke, N. (2024). Bernstein-based estimation of the cross ratio function. *Statistics* 58: 230—246.
Anderson, J.E., Louis, T.A., Holm, N.V., and Harvald, B. (1992). Time-dependent association measures for bivariate survival distributions. *J. Am. Stat. Assoc.* 87: 641—650.
Clayton, D. (1978). A model for association in bivariate life time tables and its application in epidemiological studies of familial tendency in chronic disease incidence. *Biometrika* 65: 141—151.
Dabrowska, M. (1988). Kaplan—Meier estimate on the plane. *Ann. Stat.* 16: 1475—1489.
Dib, K., Bouezmarni, M.B., and Kitouni, A. (2021). Nonparametric bivariate distribution estimation using Bernstein polynomials under right censoring. *Commun. Stat. Theor. Methods* 50: 5574—5584.
Fan, J., Hsu, L., and Prentice, R.L. (2000). Dependence estimation over a finite bivariate failure time region. *Lifetime Data Anal.* 6: 343—355, https://doi.org/10.1023/a:1026557315306.
Fang, B., Guntuboyina, A., and Sen, B. (2021). Multivariate extensions of isotonic regression and total variation denoising via entire monotonicity and Hardy-Krause variation. *Ann. Stat.* 49: 769—792.
Geerdens, C., Acar, E.F., and Janssen, P. (2017). Conditional copula models for right-censored clustered event time data. *Biometrics* 19: 247—262.
Geerdens, C., Janssen, P., and Veraverbeke, N. (2016). Large sample properties of nonparametric copula estimators under bivariate censoring. *Statistics* 50: 1036—1055.
Hu, T., Lin, X., and Nan, B. (2014). Cross-ratio estimation for bivariate failure times with left truncation. *Lifetime Data Anal.* 20: 23—37.
Hu, T., Nan, B., Lin, X., and Robins, J.M. (2011). Time-dependent cross ratio estimation for bivariate failure times. *Biometrika* 98: 341—354.
Huster, W.J., Brookmeyer, R., and Self, S.G. (1989). Modelling paired survival data with covariates. *Biometrics* 45: 145—156.
Janssen, P., Swanepoel, J., and Veraverbeke, N. (2012). Large sample behavior of the Bernstein copula estimator. *J. Stat. Plann. Inference* 142: 1189—1197.
Janssen, P., Swanepoel, J., and Veraverbeke, N. (2014). A note on the asymptotic behavior of the Bernstein estimator of the copula density. *J. Multivar. Stat.* 124: 480—487.
Janssen, P., Swanepoel, J., and Veraverbeke, N. (2016). Bernstein estimation for a copula derivative with application to conditional distribution and regression functionals. *Test* 25: 351—374.
Kaplan, E. and Meier, P. (1958). Nonparametric estimation from incomplete observations. *J. Am. Stat. Assoc.* 53: 457—481.
Kendall, M.G. (1948). *Rank correlation methods*. Charles Griffin & Company, London.
Kim, Y. and Lee, N. (2021). Time-dependent association for bivariate interval censored data. *Jpn. J. Stat. Data Sci.* 4: 1247—1262.
Lin, D. and Ying, Z. (1993). A simple nonparametric estimator of the bivariate survival function under univariate censoring. *Biometrika* 80: 573—581.
Nan, B., Lin, X., Lisabeth, L.D., and Harlow, S.D. (2006). Piecewise constant cross-ratio estimation for association of age at a marker event and age at menopause. *J. Am. Stat. Assoc.* 101: 65—77.
Nelsen, R.B. (2007). *An introduction to copulas*. Springer Science & Business Media, New York.
Oakes, D. (1989). Bivariate survival models induced by frailties. *J. Am. Stat. Assoc.* 84: 487—493.
Plumb, A.P., Swan, A.V., Chignell, A.H., and Shilling, J.S. (1982). A comparative trial of xenon arc and argon laser photocoagulation in the treatment of proliferate diabetic retinopathy. *Br. J. Ophthalmol.* 66: 213—218.
Sklar, A. (1959). Fonctions de répartition à n dimensions et leurs marges. *Pub. Inst. Stat. Univ. Paris* 8: 229—231.
Spearman, C. (1904). The proof and measurement of association between two things. *Am. J. Psychol.* 15: 72—101.
Sun, J. (2006). *The statistical analysis of interval-censored failure time data*. Springer, New York.

Supplementary Material: This article contains supplementary material (https://doi.org/10.1515/demo-2025-0023).